Aerospace Science and Technology 112 (2021) 106589

Contents lists available at ScienceDirect

Aerospace Science and Technology

www.elsevier.com/locate/aescte

The application of support vector regression and mesh deformation technique in the optimization of transonic compressor design

Handuo Hu, Jianyang Yu *, Yanping Song, Fu Chen

Harbin Institute of Technology, Heilongjiang, People's Republic of China

ARTICLE INFO

Article history:
Received 11 July 2020
Received in revised form 7 December 2020
Accepted 12 February 2021
Available online 18 February 2021
Communicated by Yongle Du

Keywords:
Transonic compressor
Optimization design
Mesh deformation
Support vector regression
Latin hypercube sample
Surrogate model

ABSTRACT

With the development of modern aero-engine, the compressor is required to achieve higher performance such as transonic operation, high stage pressure ratio and efficiency. At present, the traditional blade design methods have the disadvantage of highly relying on designer's experience and heavy computational burden. In order to reduce design variables used to define blade geometry, the present work introduces the Free-Form Deformation technique. It can achieve high degree-of-freedom deformation and update mesh and geometry simultaneously. To further alleviate computational cost, the Support Vector Regression surrogate model is adopted to replace the time-consuming numerical simulation. It performs well in small sample learning problems. On this basis, a surrogate-based optimization design framework is established by combining the Advanced Latin hypercube sample and NSGA-II multi-objective genetic algorithm. Then an aerodynamic optimization of the transonic NASA Rotor 37 is conducted as a validation. The results show that the pressure ratio and isentropic efficiency are increased by 4.2% and 2.5%, respectively. The optimized shape sweeps forward with a slight increase in twist angle, and shock loss is reduced effectively. Compared with traditional optimization method, the proposed framework can improve the optimization efficiency by decreasing design variables and training samples.

1. Introduction

Modern advanced aero-engines are developed towards high thrust-weight ratio, large stability margin and low specific fuel consumption [1]. As one of the three key components, compressor has been pursued to achieve high stage pressure ratio with no degradation in efficiency. This pushes the operating conditions to transonic regime, leading to complicated flow structures characterized by shock wave-boundary layer interaction, corner separation and leakage vortex. These concurring three-dimension flow effects not only influence the efficiency, but also have impact on stall and compressor surge, presenting challenges to the design of compressor [2]. After years of development, high fidelity Computational Fluid Dynamics (CFD) has been widely used in capturing complex flow patterns. With the benefit of advances in numerical methods and computational capacities, it is possible to carry out optimization extensively in the progress of designing state-of-the-art transonic compressor.

Traditional optimization design method has the disadvantages of relying on designer's experience, difficult to achieve the optimal solution and high cost. The last two decades have witnessed great development of numerical aerodynamic optimization method, which is based on CFD simulation and numerical optimization theory. In this method, geometry parameters are taken as design variables. Global performance of compressor, which is obtained from CFD model, is calculated as objective function. Then numerical optimization with constraints is performed to get the optimal value of objective function, as well as the optimal blade geometry. By this, the design progress can be transformed into aerodynamic optimization. Even though, thousands of CFD computations are still needed to obtain the optimal solution [3].

To alleviate the computational burden, surrogate-based optimization (SBO) strategy is getting more and more popular [4]. In this approach, surrogate model is constructed using samples generated from high-fidelity CFD simulation. The model can provide a low-cost while accurate prediction of aerodynamic performance [5,6]. However, on the one hand, a great number of design variables are necessary to allow enough shaping freedom and to obtain global optimal solution [7]. On the other hand, the number of samples directly influences the model accuracy and thereby the optimization results, according to the varying degrees of the curse of dimensionality. Siller et al. [8] carried out a multi-objective optimization with 231 design variables and calculated 1250 geometries

* Corresponding author.
E-mail address: yujianyang@hit.edu.cn (J. Yu).

https://doi.org/10.1016/j.ast.2021.106589
1270-9638/

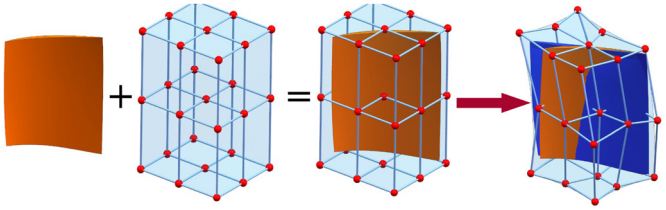

Fig. 1. Illustration of FFD deformation.

in total. A gain of 2.5% isentropic efficiency has been achieved, with slight increase of the stall margin. Although the results were impressive, it took about two months' calculation on 130 CPUs, indicating a heavy computational burden on generating samples. As a comparison, Shahpar et al. [9] used a fewer 30 engineering blade parameters and achieved 1.9% efficiency increase after 331 CFD simulations. It is worth noting that the choke mass flow was unexpectedly reduced, meaning that the lack of shaping freedom failed to deal with the compromise between multiple objectives. In conclusion, the optimization design efficiency can be significantly improved by applying efficient parameterization method and surrogate model. The former can precisely define geometry with relatively few parameters, and the latter can achieve high model accuracy using limited samples. Thus the cost on model training and numerical optimization is reduced.

The present work introduces the Free-Form Deformation (FFD) technique into the process of aerodynamic optimization. It would provide a more efficient way in parameterizing blade geometry and generating CFD mesh. To further alleviate the computational burden, the Support Vector Regression (SVR) surrogate model is adopted to build the objective function. It is characterized by performing well in small sample learning problems. Finally, a surrogate-based compressor blade optimization design framework is established by combining the advanced Latin hypercube sampling and NSGA-II multi-objective genetic algorithm. Then an aerodynamic optimization of the transonic NASA Rotor 37 is conducted. The optimal shape is present and results are analyzed in detail.

2. Methodology

2.1. Free Form Deformation

An efficient parameterization method in optimization design should promise an accurate geometry description with high degree deforming freedom [10]. To avoid the curse of dimensionality, it should also keep the number of design variables as low as possible. Thus Free Form Deformation (FFD) technique is adopted in this work as it achieves a good trade-off between deforming flexibility and number of parameters.

The FFD technique was presented by Sederberg and Parry [11], based on concept of forced deformation of elastic bodies. As shown in Fig. 1, the object to be deformed is firstly embedded in a control volume, which is defined by a grid of control points. Then a mapping from geometry coordinates to parameter space is established, and the local coordinates in parameter space are calculated. This process is called "freezing", since the local coordinates keep unchanged in the subsequent operation. By moving the position of control points, the shape of control volume is changed according to the specific basis function. With the deformed control volume, the new positions of geometry points are calculated, thereby achieving the deformation of the object.

Mathematically, any point $\vec{X}$ in the local coordinate system has $(s,\ t,\ u)$ coordinates such that

$$\vec{X}(s,t,u) = \vec{P}_0 + s\vec{S} + t\vec{T} + u\vec{U} \tag{1}$$

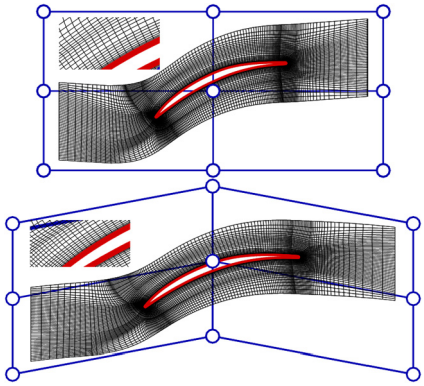

Fig. 2. Illustration of 2-D mesh deformation.

where $\vec{P}_0$ is the selected origin of control volume, and $\vec{S}$, $\vec{T}$, $\vec{U}$ are the three direction vectors. For parallelepiped control volume, the $(s,\ t,\ u)$ coordinates can be solved using linear algorithm from Eq. (2), while Newton approximation can deal with any type of control volume [12].

$$s = \frac{\vec{T}\times\vec{U}(\vec{X}-\vec{P}_0)}{\vec{T}\times\vec{U}\cdot\vec{S}},\ t = \frac{\vec{S}\times\vec{U}(\vec{X}-\vec{P}_0)}{\vec{S}\times\vec{U}\cdot\vec{T}},\ u = \frac{\vec{S}\times\vec{T}(\vec{X}-\vec{P}_0)}{\vec{S}\times\vec{T}\cdot\vec{U}} \tag{2}$$

Suppose we impose l+1, m+1, n+1 control points in the $\vec{S}$, $\vec{T}$, $\vec{U}$ directions respectively, and use $\vec{P}_{ijk}$ to represent them. Then an arbitrary point $\vec{X}$ can be expressed as a linear combination of $\vec{P}_{ijk}$:

$$\vec{X}(s,t,u) = \sum_{i=0}^{l}\sum_{j=0}^{m}\sum_{k=0}^{n}\vec{P}_{ijk}R_i(s)R_j(t)R_k(u) \tag{3}$$

where $R(\cdot)$ is the basis function. In this work the Bernstein basis function is adopted:

$$R_i(s) = B_l^i(s) = C_l^i(1-s)^{l-i}s^i \tag{4}$$

To achieve deformation, suppose the control points $\vec{P}_{ijk}$ are moved to $(\vec{P}_{ijk}+\Delta\vec{P}_{ijk})$. Accordingly, geometry points $\vec{X}$ become $(\vec{X}+\Delta\vec{X})$, and Eq. (3) still holds:

$$(\vec{X}+\Delta\vec{X}) = \sum_{i=0}^{l}\sum_{j=0}^{m}\sum_{k=0}^{n}(\vec{P}_{ijk}+\Delta\vec{P}_{ijk})R_i(s)R_j(t)R_k(u) \tag{5}$$

So we can get the displacement $\Delta\vec{X}$:

$$\Delta\vec{X}(s,t,u) = \sum_{i=0}^{l}\sum_{j=0}^{m}\sum_{k=0}^{n}\Delta\vec{P}_{ijk}R_i(s)R_j(t)R_k(u) \tag{6}$$

The above equation is valid for all geometry points in the control volume. In this way we can obtain the deformed object. In fact, FFD method focuses on overall deformation and coordination. The influence of moving control points will spread to the whole blade with varying degrees. In this way FFD method can achieve flexible deformation even when control points move a lot.

It is worth noting that FFD deformation directly operates at each geometry point in the control volume. This feature makes it possible to simultaneously update blade geometry and computational mesh, thus avoiding repeated mesh generation. The FFD mesh deformation illustration of a 2-D blade and passage is shown in Fig. 2. The deformed mesh maintains the same topology as the original. The mesh quality of the boundary layer meets the requirements of CFD simulation.

2.2. Support Vector Regression

In recent years, machine learning-based method has been applied on many fields successfully [13,14]. As one of them, Support Vector Machine (SVM) adopts the latest achievements of statistical learning theory. Base on the Structural Risk Minimization (SRM) principle, it has excellent generalization ability. Moreover, the use of kernel function avoids the Curse of Dimensionality problem. Because in this way, the inner product in high-dimensional feature space becomes irrelevant to the dimension of variables.

Support Vector Machine method was originally used to solve classification problems [15]. Later, its idea and method were extended to solve regression problem, which is called Support Vector Regression (SVR). Compared with classification problem, when using SVR to solve regression problem, the return value is not discrete like 1 or -1, but continuous real number.

For the linear regression problem (Ref. [16]), suppose a training sample is $\{(x_1, y_1), (x_2, y_2), \ldots, (x_n, y_n)\}$, and the fitting form is:

$$f(x) = \omega \cdot x + b \tag{7}$$

Assuming a small positive ε, if all samples can be fitted with the accuracy of ε, i.e., $|y_i - f(x_i)| \le \varepsilon$, the fitting can be considered lossless. Taking into account the allowable fitting error, we introduce the relaxation factors ξ_i, ξ_i^*. In general, the goal is to construct an optimal hyperplane with maximal margin $1/\|\omega\|$ and minimal fitting loss $\sum_{i=1}^{n}(\xi_i + \xi_i^*)$. Moreover, these two objectives can be combined by introducing penalty factor C. Thus the hyperplane can be found by solving the following optimization problem:

$$\min \quad \frac{1}{2}\|\omega\|^2 + C\sum_{i=1}^{n}(\xi_i + \xi_i^*) \tag{8}$$

$$\text{S.T.} \quad \begin{aligned} & y_i - \omega \cdot x_i - b \le \varepsilon + \xi_i \\ & \omega \cdot x_i + b - y_i \le \varepsilon + \xi_i^* \\ & \xi_i,\ \xi_i^* \ge 0 \quad i = 1, 2, \cdots, n \end{aligned} \tag{9}$$

In this way the model ε-SVR is thus obtained. Since the size of ε is hard to estimate in advance, a new factor ν is introduced. The $\nu \in (0, 1]$ describes the influence of ε and is easy to give, so that ε can be obtained during the calculation. Thereby developed the ν-SVR model. For the ν-SVR model, the corresponding optimization problem can be rewritten as:

$$\min \quad \frac{1}{2}\|\omega\|^2 + \frac{C}{n}\sum_{i=1}^{n}(\nu\varepsilon + \xi_i + \xi_i^*) \tag{10}$$

$$\text{S.T.} \quad \begin{aligned} & y_i - \omega \cdot x_i - b \le \varepsilon + \xi_i \\ & \omega \cdot x_i + b - y_i \le \varepsilon + \xi_i^* \\ & \xi_i,\ \xi_i^* \ge 0 \quad i = 1, 2, \cdots, n \end{aligned} \tag{11}$$

To solve the above problem, we apply Lagrange multiplier method to convert it into its dual problem. Lagrange multipliers α_i, α_i^* are introduced, and the transformed optimization problem becomes:

$$\min \quad \frac{1}{2}\sum_{i,j=1}^{n}(\alpha_i^* - \alpha_i)(\alpha_j^* - \alpha_j)\langle x_i, x_j\rangle - \sum_{i=1}^{n} y_i(\alpha_i^* - \alpha_i) \tag{12}$$

$$\text{S.T.} \quad \begin{aligned} & \sum_{i=1}^{n}(\alpha_i - \alpha_i^*) = 0 \\ & \sum_{i=1}^{n}(\alpha_i + \alpha_i^*) \le C \cdot \nu \\ & 0 \le \alpha_i, \alpha_i^* \le \frac{C}{n} \quad i = 1, 2, \cdots, n \end{aligned} \tag{13}$$

α_i, α_i^* are obtained after solving, and the established linear regression model is:

$$f(x) = \sum_{i=1}^{n}(\alpha_i - \alpha_i^*)\langle x, x_i\rangle + b \tag{14}$$

In practice, nonlinear fitting is more often the case. For this kind of problem, SVR tries to fit the sample set in the high dimensional feature space. A nonlinear transformation $\varphi(\cdot)$ maps the original sample set to the high dimensional feature space. However, the inner product $\langle\varphi(x), \varphi(x_i)\rangle$ may become complex in high dimensional space. Thus it is replaced by kernel function $K(x, x_i)$ corresponding to the original low-dimensional space. According to functional theory, they are equivalent and the replacement is reasonable. By this way, the regression model under nonlinear problems can be obtained:

$$f(x) = \sum_{i=1}^{n}(\alpha_i - \alpha_i^*)K(x, x_i) + b \tag{15}$$

Commonly used kernel functions include linear kernel functions, polynomial kernel functions, radial basis (RBF) kernel functions, and Sigmoid kernel functions. There are also mixed kernel functions combining the characteristics of different kernel functions. The type of kernel function determines the mapping form from sample space to high dimensional feature space, which has a significant impact on the prediction accuracy of model. Therefore, reasonable selection of kernel function should be made according to the feature of problems and samples. When prior knowledge is insufficient, the radial basis (RBF) kernel function is generally preferred, which has a good adaptability. Therefore, this paper adopts the radial basis (RBF) kernel function:

$$K(x, x_i) = \exp\{-\gamma\|x - x_i\|^2\}, \quad \gamma > 0 \tag{16}$$

Once the kernel function is determined, the model parameters that need to be adjusted are also determined. These include the penalty factor C for the generalization ability of the control model, RBF kernel function parameter γ for the scope of the control function, and model factor ν for the number of support vectors. It is simple to use grid search method for parameter optimization, but the computation cost will increase along with the number and range of parameters. Therefore, this paper uses genetic optimization algorithm to achieve the optimal parameter combination. For the optimization process, model parameters are taken as design variables, and prediction error on the test set as objective function.

2.3. Benchmark function test

This section will verify the prediction ability of the above SVR model. This is done by four higher-order nonlinear standard test functions [17], as shown in Eq. (17)∼(20).

$$f_{SC}(x) = 4x_1^2 - \frac{21}{10}x_1^4 + \frac{1}{3}x_1^6 + x_1x_2 - 4x_2^2 + 4x_2^4,\ x_1, x_2 \in [-2, 2] \tag{17}$$

$$\begin{aligned} f_{GP}(x) = {} & [1 + (x_1 + x_2 + 1)^2(19 - 14x_1 + 3x_1^2 \\ & - 14x_2 + 6x_1x_2 + 3x_2^2)]\times \\ & [30 + (2x_1 - 3x_2)^2(18 - 32x_1 + 12x_1^2 + 48x_2 \\ & - 36x_1x_2 + 27x_2^2)] \\ & x_1, x_2 \in [-2, 2] \end{aligned} \tag{18}$$

Table 1
Benchmark test RAAE results of the SVR and BPNN.

Test Function	Variable Number n_v	$30n_v$		$20n_v$		$10n_v$	
		SVR	BPNN	SVR	BPNN	SVR	BPNN
SC	2	0.78%	0.19%	3.11%	9.10%	5.22%	10.44%
GP	2	2.46%	13.06%	5.37%	19.26%	22.16%	35.33%
HN	6	29.34%	76.57%	37.26%	75.38%	43.32%	87.23%
F16	16	4.81%	70.14%	11.28%	95.46%	14.07%	113.45%

$$f_{HN}(x) = -\sum_{i=1}^{4} c_i \exp\left[-\sum_{j=1}^{6} \alpha_{ij}(x_j - p_{ij})^2\right], \quad x_j \in [0,1] \tag{19}$$

$$f_{F16}(x) = \sum_{i=1}^{16}\sum_{j=1}^{16} a_{ij}(x_i^2 + x_i + 1)(x_j^2 + x_j + 1), \quad i, j = 1, \ldots, 16, \quad x_i \in [-1, 0] \tag{20}$$

The function parameters c_i and a_{ij} can be obtained from Ref. [17].

In order to study the relationship between the model accuracy and sample size, samples of 10 times, 20 times, and 30 times the number of variables n_v are obtained as training sets; to accurately assess the accuracy of the model, another sample with 100 times n_v is used as the test set. Latin Hypercube sampling method is adopted during the above process. For the model accuracy evaluation criterion, we choose relative average absolute error RAAE calculated as Eq. (21).

$$\text{RAAE} = \frac{\sum_{i=1}^{n_t} |y_i - \hat{y}_i|}{n_t \cdot \text{STD}}; \quad \text{STD} = \sqrt{\frac{1}{n_t - 1}\sum_{i=1}^{n_t}(y_i - \hat{y}_i)^2} \tag{21}$$

For each benchmark function the above modeling and evaluating process is repeated 10 times to reduce randomness, and the average of RAAE is taken as final performance. As a comparison, another commonly used machine learning method, Back Propagation Neural Network (BPNN), is performed in the same way. The analysis of the results is as follows in Table 1.

The test results are shown in Table 1. It can be seen that SVR and BPNN can reach a similar level of prediction accuracy when samples are enough. With the training set size decreasing, both prediction errors inevitably increase. However, SVR model has an obviously less increasing range than BPNN's. This difference indicates that SVR is less sensitive to sample size. With this feature, SVR has a significant advantage when dealing with small sample problems, which are common in aerodynamic optimization design.

3. SBO design framework

On the basis of the previous study, a surrogate-based-optimization design framework is proposed in this paper, as shown in Fig. 3. Firstly, the original geometry is parameterized using Free-Form Deformation method. Then advanced Latin hypercube design is applied to generate certain amount of samples in the design space. To obtain the response values on these samples, FFD method updates geometry and mesh simultaneously and CFD simulation calculates aerodynamic parameters. Thus a database is established and ν-SVR with RBF kernel function is trained as the surrogate model. Having validated model accuracy, NSGA-II multi-objective algorithm can be performed and finally the optimal design is obtained.

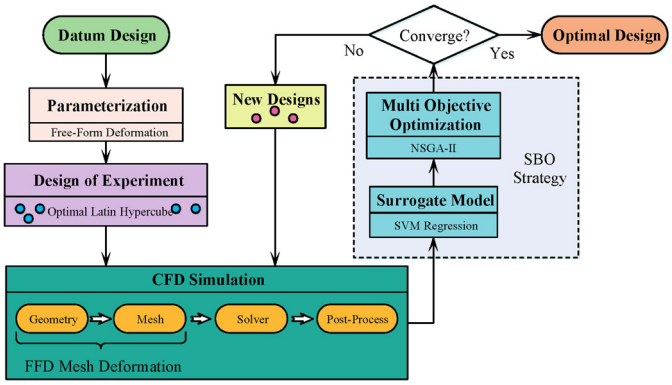

Fig. 3. Flowchart of SBO design framework.

Table 2
Design intent of NASA Rotor 37.

Parameter	Value
Mass flow	20.19 kg/s
Rotational speed	17188.7 rpm
Pressure ratio	2.106
Inlet hub-tip ratio	0.7
Inlet tip relative Mach number	1.4
Inlet hub relative Mach number	1.13
Tip solidity	1.288
Rotor aspect ratio	1.19
Number of rotor blades	36

4. Rotor 37 optimization

As a demonstration of the performance of the proposed SBO design framework, this section performed an optimization progress towards NASA Rotor 37. A numerical model is firstly established, and its accuracy is validated by comparing CFD with experimental results. Then after parameterizing geometry using FFD method, a multi-objective optimization is carried out. Finally, the results are analyzed in detail by comparing the original and optimized blade profile, flow field and performance including isentropic efficiency and pressure ratio.

4.1. Design intent

Rotor 37 is a transonic compressor rotor designed by NASA Lewis Research Center in 1970s. It has strong shock wave-boundary layer interaction, tip leakage vortex, end wall separation and other typical flow characteristics of transonic compressor. Reid et al. [18] has conducted detailed experimental measurements on the flow field. Therefore, Rotor 37 is widely used for the analysis of experimental and numerical models as well as the verification of the optimization design method. The main parameters of Rotor 37 are shown in Table 2, and the meridional view is shown in Fig. 4.

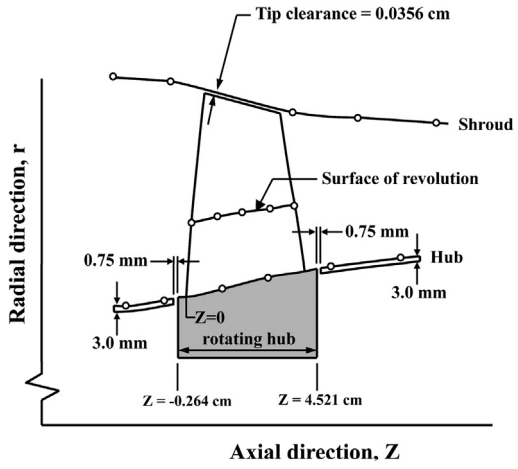

Fig. 4. Meridional view of Rotor 37.

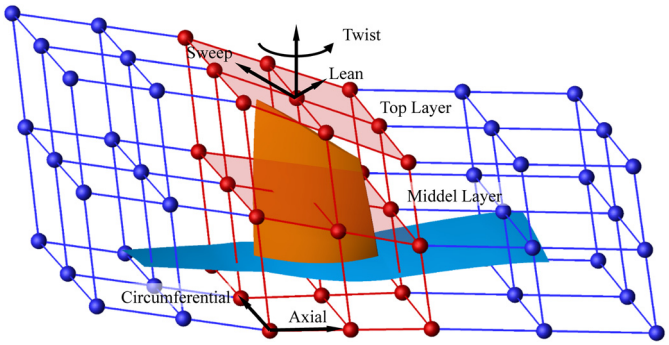

Fig. 5. FFD control volume of Rotor 37 CFD domain (points to be moved are marked in red). (For interpretation of the colors in the figure(s), the reader is referred to the web version of this article.)

Table 3
Parameters' range of control Points.

Parameters	Range
Movements	±25% point to point distance
Sweep	±15% tip chord
Lean	±5% tip chord
Twist	±1.5 degree

4.2. Parameterization

Around the computation domain, a segmented FFD control body is created, as shown in Fig. 5. The inlet and outlet control bodies (blue) remain unchanged during updating process. The control body around the blade (red) is composed of a grid of $3 \times 3 \times 3$ control points. By moving these 27 control points the blade can be deformed. Related to the movements of control points, a total of 60 design variables are set as follows: the axial and circumferential movements of each control point are defined respectively, corresponding to 54 design variables; three forms of overall movements including sweeping, bowing and twisting of the middle and top layers are defined, corresponding to the remaining 6 variables. The moving range of 27 control points is showed as Table 3. Baert et al. [19] selected similar design variables.

4.3. Numerical model

The mesh used to validate the numerical model is generated by TurboGrid. In order to ensure the mesh orthogonality near the leading edge (LE) and the trailing edge (TE), an 'O' block mesh is applied around the blade. For the inlet and outlet part, two 'H' blocks are defined. The block at the 0.356 mm tip clearance creates a butterfly topology, and interfaces are set to match with the neighboring blocks. In order to ensure numerical results independent of mesh size, three cases of different grid levels are set and calculated. The grid number and choked flow rate of each case are listed in Table 4. The results show that the medium level case can achieve almost the same solution as the fine level, which is very close to the experimental value 20.93±0.14 kg/s. Fig. 6 shows the calculated isentropic efficiency of three cases. Over most flow rate ranges, the medium level keeps consistent with the fine, despite slight difference at near stall.

Table 4
Node number and numerical results of grid independency test.

Cases	Node number	Choked flow rate (kg/s)
Coarse	450,000	20.45
Medium	650,000	20.94
Fine	850,000	20.94

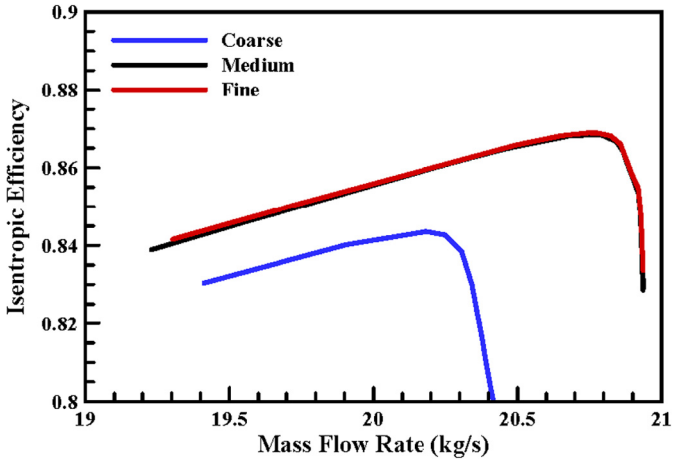

Fig. 6. Isentropic efficiency of grid independency test.

As a result, a high-quality mesh of 650,000 grid points is finally selected for CFD simulation and optimization. Fig. 7 shows the grid point distribution on S1 stream surface and in radial direction, together with regions at LE, TE and shroud tip.

The CFD simulation is performed on ANSYS CFX to solve the steady RANS equation. The boundary conditions are set as experimental stations. At the inlet, a radial profile of total pressure and temperature is specified. In order to simulate different flow condition, the static pressure at average radius is controlled at the outlet. Each wall is set as non-slip and adiabatic. The hub and blade are treated as rotating wall with 17188.7 rpm, while the shroud keeps stationary. Since only a single channel is meshed, periodic boundaries are used in circumferential direction to represent full annulus flow. For the current study, $k-\varepsilon$ is adopted as turbulence model.

The validity of this numerical model is demonstrated by comparing with experimental data and simulation results taken from NASA Ameri's work [20].

As shown in Fig. 8, the pressure ratio keeps consistent with experiment on most mass flow rate, while isentropic efficiency is around 2% less than experimental data in average. This agrees with other researchers' work, according to the AGARD blind test [21]. Fig. 9 shows the radial distribution of pressure ratio and efficiency at near peak condition. Both parameters' radial trends have reasonable agreement over most blade span.

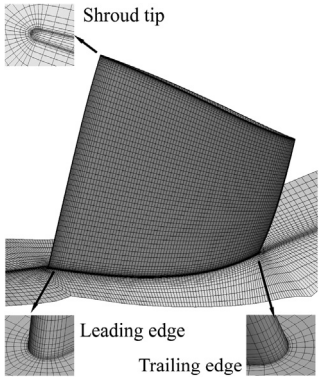

Fig. 7. Illustration of computational mesh.

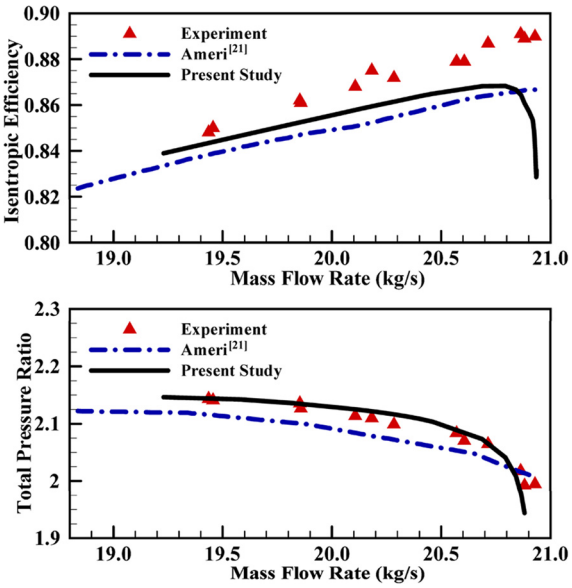

Fig. 8. Comparison of simulation and experimental data on the overall performance.

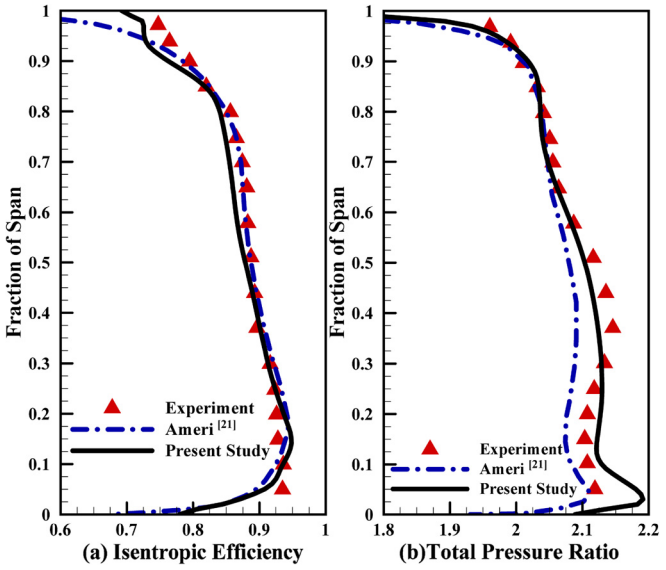

Fig. 9. Comparison of simulation and experimental data at near peak point across span.

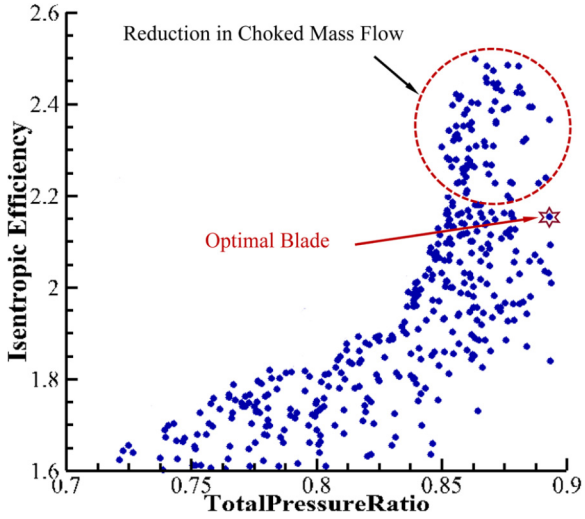

Fig. 10. Pareto front of pressure ratio and efficiency obtained by NSGA-II.

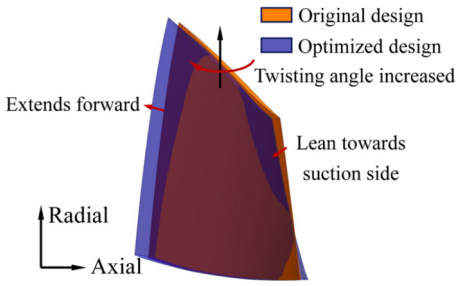

Fig. 11. Comparison of original and optimal 3-D blade geometry.

4.4. Optimization strategy

On the basis of the verified numerical model, a certain number of samples are generated by applying the advanced Latin hypercube sampling (LHS) method. For each sample, the deformed geometry as well as mesh are updated by FFD free mesh deformation. Then the aerodynamic performance is evaluated by CFD simulation, including total pressure ratio, isentropic efficiency and mass flow rate. In this way, a database with design variables and performance parameters is established. Using the information in the database, the SVR model is trained, and the model accuracy is verified by Leave-One-Out (LOO) method. Under the condition that the prediction error is controlled within 10%, the SVR model can replace high-fidelity CFD simulation. Finally, the NSGA-II multi-objective optimization is applied aiming at maximizing pressure ratio and efficiency while keeping choked mass flow rate no less than 95% original level.

For the Rotor 37, a total of 750 samples have been generated from LHS method. After CFD simulations, 486 samples are usable for the subsequent SBO optimization. Among the failed samples, 105 have bad mesh quality, and 159 fail to converge or achieve unreasonable results. All usable samples serve as training set for ν-SVR model. Through LOO validation, the model error is evaluated as 8.66%, meeting the requirement to predict performance of new geometry. Having taken a month of run-time in total, the NSGA-II multi-objective optimization achieves the final Pareto set, as shown in Fig. 10. After CFD verification and comparison, the optimal results of optimization are selected.

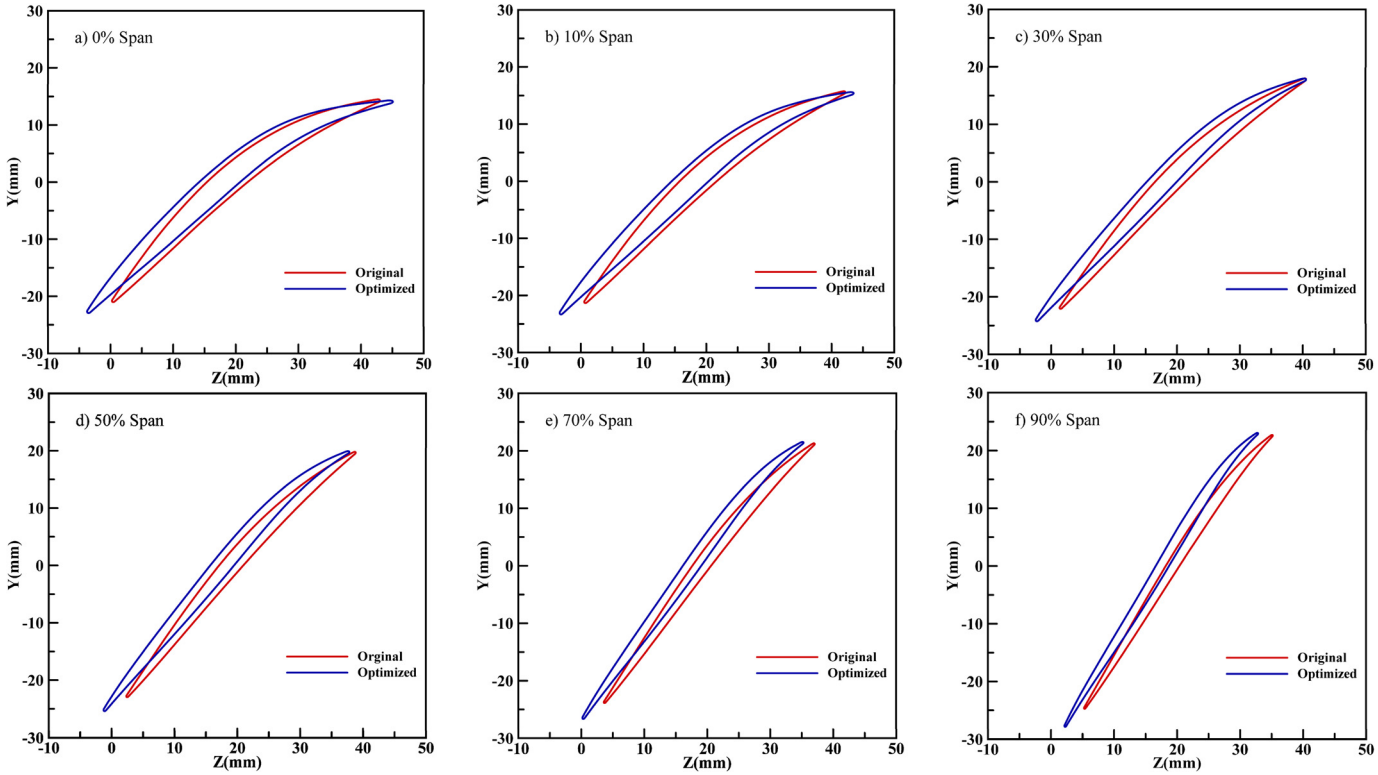

Fig. 12. Comparison of original and optimal 2-D blade sections.

5. Results and discussion

5.1. Optimized geometry

Firstly, a three-dimensional illustration of the original and optimized blade geometry is shown in Fig. 11 intuitively. In more details, the blade profiles at different sections are compared in Fig. 12. It can be seen that, the leading edge (LE) sweeps forward significantly all along the span. As a result, the chord length expands. Over the upper half of blade, the camber line shifts towards suction side. The twisting angle increased slightly at shroud tip and near hub.

5.2. Flow field characteristics

Because of the above blade geometry deformation, the flow characteristics inside rotor have been affected. The alleviation of shock wave and flow separation can be seen in Fig. 13. Since the suction side goes deeper into flow channel, a re-acceleration occurs right after the passage shock. With an increased Mach number after wave, the shock is weakened and loss is reduced.

The re-acceleration zone can be identified in Fig. 14. Compared with the original front-loaded blade, the loading on the optimized blade has shifted rearward. Meanwhile, the compression of flow channel delays the flow separation on the suction surface. The separation and weak region also shrinks with less low momentum fluid. The change of entropy product shown in Fig. 15 confirms the reduction of flow loss.

The change of shock wave structure can be seen in Fig. 16. From 30% span onwards, the original strong normal shock has been transformed into weakened oblique shock. The alleviation of passage shock plays a positive role in reducing total pressure loss.

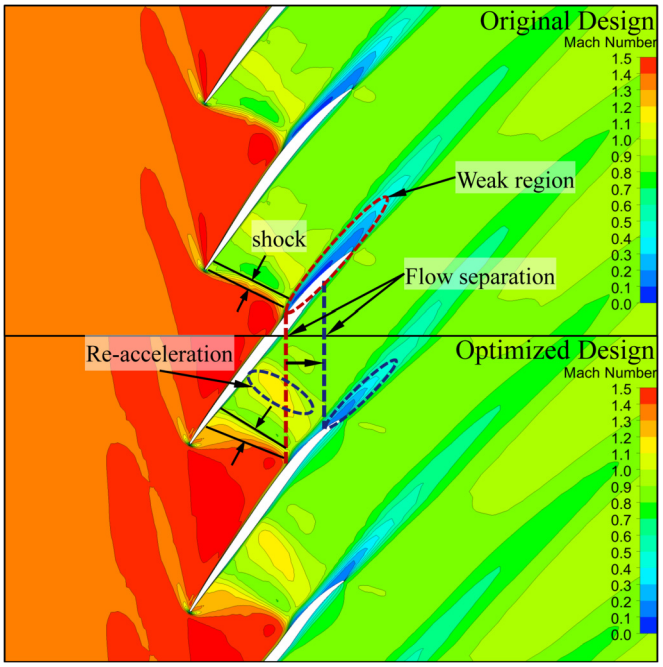

Fig. 13. Comparison of original and optimized design on Mach number at 70% blade span.

5.3. Performance analyses

The improvement of the flow field benefits the overall aerodynamic performance of rotor. In order to properly assess the off-design characteristics of the optimized blade, several CFD simulations are carried out from near stall to choke point. The result is shown in Fig. 17. At the design point, the total pressure ratio is increased by 4.2%, and the isentropic efficiency by 2.5%. It

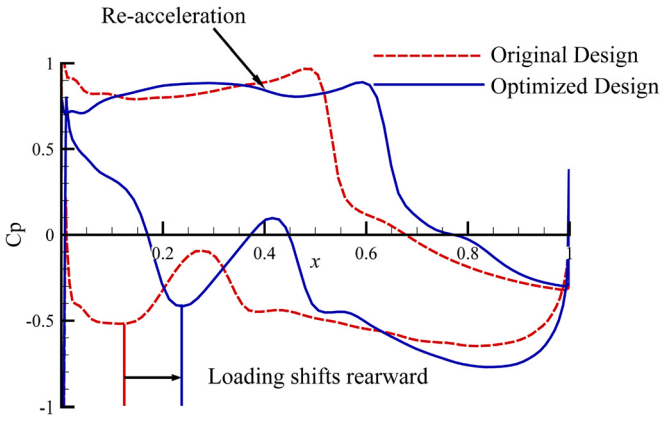

Fig. 14. Comparison of surface pressure coefficient at 70% blade span.

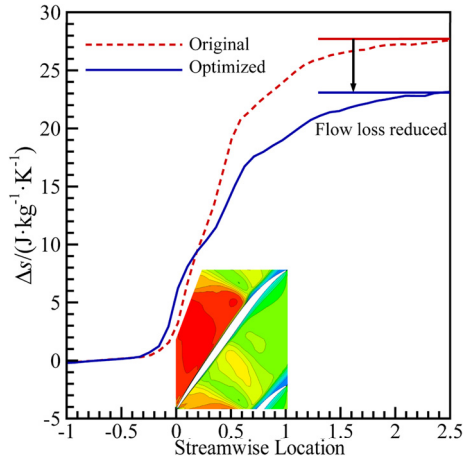

Fig. 15. Comparison of original and optimized design on entropy product at 70% blade span.

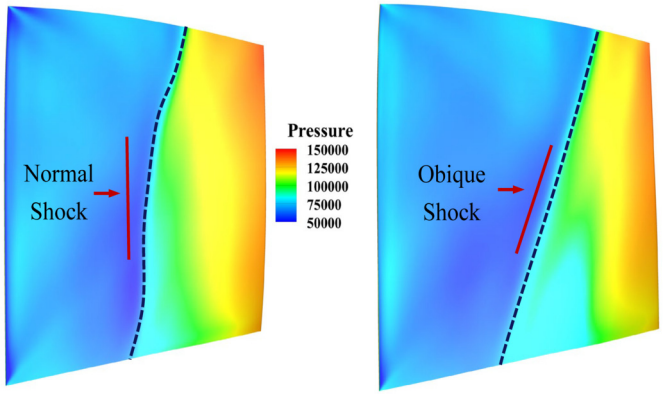

Fig. 16. Comparison of original and optimized static pressure at the suction side.

is noticeable that the choke margin also improved by 2.7%, while many other studies (Ref. [9,19,22]) have to face a varying degree of reduction. The expansion of surge margin improves compressor stability and ability to do work. The above analyses validate that the proposed method can achieve impressive results with a less requirement on the quantity of design variables and training samples.

6. Conclusions

In this paper, FFD free mesh deformation is used to parameterize blade geometry and flow channel. To alleviate computational

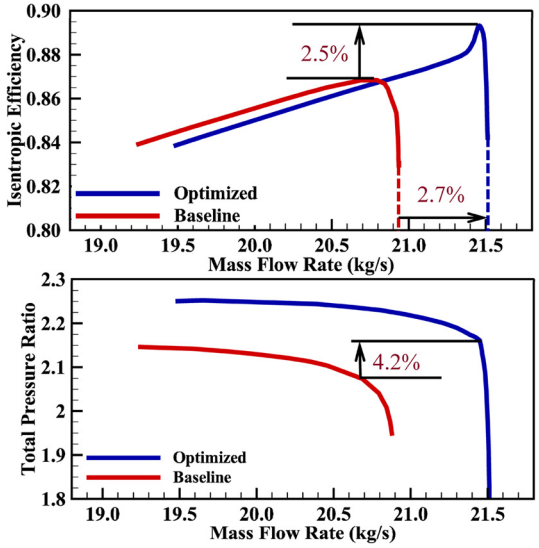

Fig. 17. Comparison of optimized and original on the overall performance.

burden, SVR surrogate model is adopted to replace CFD simulation. Combined with improved Latin hypercube sampling and NSGA-II multi-objective optimization algorithm, a SBO design framework is established. The effectiveness of the proposed method is verified by the redesign of the transonic compressor Rotor 37, and the following conclusions are drawn:

FFD free-form deformation technology can realize large-degree-of-freedom deformation with fewer design variables. Moreover, the deformation directly acts on all points embedded in control body. Therefore, FFD free deformation can simultaneously update blade geometry and computational mesh. In this way it can reduce the number of design variables and avoid the re-meshing process during optimization.

SVR model can achieve the required level of prediction accuracy with relatively few training samples, thereby reducing CFD simulation calls and computational cost. The benchmark test shows that the SVR model performs better when facing small sample problem. However, to achieve high model accuracy also relies on the rational selection of kernel functions and model parameters according to actual problems.

The optimization design framework proposed in this paper can improve design efficiency by reducing the design variables and the number of training samples. The optimized blade achieves 4.2% pressure ratio and 2.5% efficiency improvement, due to the reduction of the shock and flow loss. Meanwhile the decrease of the choked mass flow rate is avoided. Based on the above results, the effectiveness of the proposed framework is validated.

Declaration of competing interest

The authors declare that they have no known competing financial interests or personal relationships that could have appeared to influence the work reported in this paper.

References

[1] H.F. Gao, E. Zio, A. Wang, G.C. Bai, C.W. Fei, Probabilistic-based combined high and low cycle fatigue assessment for turbine blades using a substructure-based kriging surrogate model, Aerosp. Sci. Technol. 104 (2020) 105957.
[2] R. Biollo, E. Benini, Recent advances in transonic axial compressor aerodynamics, Prog. Aerosp. Sci. 56 (2013) 1–18.
[3] A.I.J. Forrester, A.J. Keane, Recent advances in surrogate-based optimization, Prog. Aerosp. Sci. 45 (2009) 50–79.
[4] H. Kaya, H. Tiftikçi, Ü. Kutluay, E. Sakarya, Generation of surrogate-based aerodynamic model of an UCAV configuration using an adaptive co-Kriging method, Aerosp. Sci. Technol. 95 (2019) 105511.

[5] G. Giangaspero, D. MacManus, I. Goulos, Surrogate models for the prediction of the aerodynamic performance of exhaust systems, Aerosp. Sci. Technol. 92 (2019).
[6] J. Yu, Z. Wang, F. Chen, J. Yu, C. Wang, Kriging surrogate model applied in the mechanism study of tip leakage flow control in turbine cascade by multiple DBD plasma actuators, Aerosp. Sci. Technol. 85 (2019) 216–228.
[7] Y. Shen, W. Huang, L. Yan, T. Zhang, Constraint-based parameterization using FFD and multi-objective design optimization of a hypersonic vehicle, Aerosp. Sci. Technol. 100 (2020).
[8] U. Siller, C. Voß, E. Nicke, Automated multidisciplinary optimization of a transonic axial compressor, in: Aiaa Aerospace Sciences Meeting, 2009.
[9] S. Shahpar, A. Polynkin, V. Toropov, Large scale optimization of transonic axial compressor rotor blades, 2008.
[10] S. Menzel, M. Olhofer, B. Sendhoff, Application of free form deformation techniques in evolutionary design optimisation, in: Proceedings of 6th World Congress on Structural and Multidisciplinary Optimization, Rio de Janeiro, Brazil, 2005.
[11] T.W. Sederberg, S.R. Parry, Free-form deformation of solid geometric models, in: Proceedings of the 13th Annual Conference on Computer Graphics and Interactive Techniques, 1986, pp. 151–160.
[12] S. Coquillart, Extended free-form deformation: a sculpturing tool for 3D geometric modeling, in: Conference on Computer Graphics & Interactive Techniques, 1990, pp. 187–196.
[13] Y. Lin, J.-w. Zhang, H. Liu, Deep learning based short-term air traffic flow prediction considering temporal–spatial correlation, Aerosp. Sci. Technol. (2019).
[14] C. Che, H. Wang, Q. Fu, X. Ni, Combining multiple deep learning algorithms for prognostic and health management of aircraft, Aerosp. Sci. Technol. (2019) 105423.
[15] B.E. Boser, I.M. Guyon, V.N. Vapnik, A training algorithm for optimal margin classifier, in: Workshop on Computational Learning Theory, 1992.
[16] R. Stephan Sain, The nature of statistical learning theory, Technometrics 38 (1996) 409.
[17] M. Jamil, X.S. Yang, A literature survey of benchmark functions for global optimization problems, Int. J. Math. Model. Numer. Optim. 4 (2013) 150–194.
[18] L. Reid, R.D. Moore, Design and overall performance of four highly loaded, high speed inlet stages for an advanced high-pressure-ratio core compressor, 1978.
[19] L. Baert, P. Beaucaire, M. Leborgne, C. Sainvitu, I. Lepot, Tackling highly constrained design problems: efficient optimisation of a highly loaded transonic compressor, in: Asme Turbo Expo, 2017.
[20] A. Ameri, NASA ROTOR 37 CFD CODE validation Glenn-HT code, in: 47th AIAA Aerospace Sciences Meeting Including the New Horizons Forum and Aerospace Exposition, 2009.
[21] J. Dunham, CFD Validation for Propulsion System Components (la Validation CFD des organes des propulseurs), Cfd Validation for Propulsion System Components, 1998.
[22] C.J. Brooks, A.I.J. Forrester, A.J. Keane, S. Shahpar, Multi-fidelity design optimisation of a transonic compressor rotor, in: 9th European Conf. Turbomachinery Fluid Dynamics and Thermodynamics, 25/03/11, 2011.